ADVANCED FUNCTIONAL MATERIALS
www.afm-journal.de

Integrated Saltwater Desalination and Energy Storage through a pH Neutral Aqueous Organic Redox Flow Battery

*Camden Debruler, Wenda Wu, Kevin Cox, Brice Vanness, and T. Leo Liu**

Here, a pH neutral aqueous organic redox flow battery (AORFB) consisting of three electrolytes channels (i.e., an anolyte channel, a catholyte channel, and a central salt water channel) to achieve integrated energy storage and desalination is reported. Employing a low cost, chemically stable methyl viologen (MV) anolyte, and sodium ferrocyanide catholyte, this desalination AORFB is capable of desalinating simulated seawater (0.56 M NaCl) down to 0.023 M salt concentration at an energy cost of 2.4 W h L^{-1} of fresh water—competitive with current reverse osmosis technologies. Simultaneously, the cell delivers stored energy at 79.7% efficiency with a cell voltage of 0.85 V. Furthermore, the cell is also capable of higher current operation up to 15 mA cm^{-2}, providing 4.55 mL of fresh water per hour. Combining energy storage and water desalination into such a bifunctional device offers the opportunity to address two growing global issues from one hardware installation.

1. Introduction

Freshwater scarcity is one of the global grand challenges faced by the development of modern society (**Figure 1**, blue curve).[1–3] By the year 2025, 3.5 billion people will live in regions (especially in most populated countries) with water scarcity.[1] The most promising approach to address this challenge is to harness the vast water supply in the world's oceans (covering 97% of the total water of the planet) without impairing natural freshwater ecosystems (only 0.5% of the earth's total water).[4] Unfortunately, this water must first be pretreated to remove dissolved salts before it is usable for human consumption or agriculture. To date, reverse osmosis (RO) represents the state of the art water desalination technique with commercial installations worldwide, but the high costs (>\$0.53 m^{-3}) and high energy demand (≈3–6 W h electricity L^{-1} water production) to generate fresh water from sea water are the limiting factors for large scale implementation.[1,4] Other desalination methods including multistage flash distillation, multiple-effect distillation and solar thermal distillation are very energy intensive and are expensive for wide-spread desalination water production.[5] Electrochemical technologies including electrodialysis, capacitive deionization, and faradaic deionization offer alternative means for saltwater desalination.[6] However, due to the use of solid state electrodes in these systems, desalination capacities of capacitive devices are low and most suitable for the desalination of brackish water while faradaic deionization employing solid state electrodes suffer from slow desalination due to sluggish ion diffusions.[6] Thus, designing a more energy efficient and cost-effective system is critical to improve seawater desalination's ability and meet the growing freshwater need.

Coupled with increasing freshwater demand, the worldwide energy demand is also growing rapidly (Figure 1, red curve).[7,8] By a large margin, worldwide energy production relies on non-renewable coal and fossil fuel sources.[9] Shifting the energy production paradigm toward renewable sources like solar and wind requires advanced energy storage technology to overcome fluctuating demand and intermittent production.[10] Redox flow batteries (RFBs, **Figure 2**A) offer promising advantages over traditional electrochemical energy storage methods like lithium ion including scalability, price, and safety.[11–14] RFBs employ two redox couples in liquid form as charge storage materials for energy conversion between electrical energy and chemical energy. The cathode and anode liquid electrolytes, called catholyte and anolyte respectively, are stored in two separate reservoirs and pumped through the electrode surface of an independent electrochemical cell where electrochemical reactions take place for energy conversion (Figure 2). RFBs represent one of the most promising battery technologies currently implemented for commercial, grid-scale energy storage.[15]

By modifying the traditional two channel RFB design (Figure 2A), it is possible to harness the internal charge balancing salt flow to selectively desalinate sea water while simultaneously storing energy electrochemically. This single device is poised to address both problems of water scarcity and renewable energy storage. A three channel RFB design for coupled energy storage and desalination is shown in Figure 2B. Because of this unique cell architecture, desalination RFBs have several advantages for faradaic desalination and beyond, 1) desalination capacity can be independently increased by increasing the concentrations of active material and the size of reservoirs; 2) they can be operated at relatively high currents benefited from fast

C. Debruler, W. Wu, K. Cox, Prof. T. L. Liu
The Department of Chemistry and Biochemistry
Utah State University
Logan, UT 84322, USA
E-mail: leo.liu@usu.edu
B. Vanness
The Department of Chemistry and Biochemistry
California State University
Chico, CA 95926, USA
The ORCID identification number(s) for the author(s) of this article can be found under https://doi.org/10.1002/adfm.202000385.

DOI: 10.1002/adfm.202000385

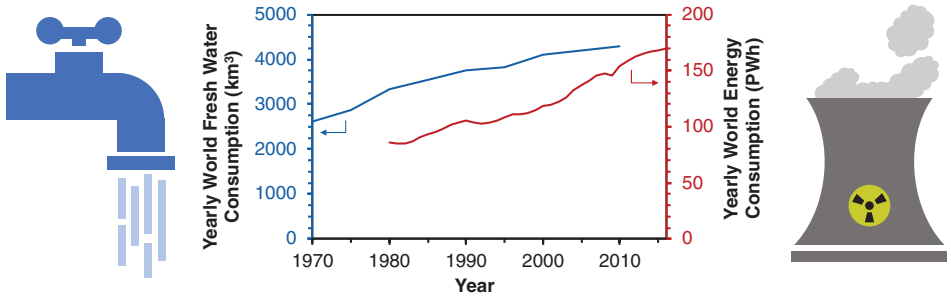

Figure 1. Plot showing the steady increase in world fresh water and energy consumptions by year. Data adapted from The Food and Agriculture Organization of the United Nations (2012), and The United States Energy Information Administration respectively (2017).

electrochemical reaction kinetics, and the solution phase active materials overcome sluggish intercalation processes found in solid state electrodes; 3) they can be easily refreshed by replacing electrolyte solutions without opening the battery framework; 4) they enable the combination of charge mismatched redox couples to construct more versatile flow battery designs, which otherwise cannot be used in traditional RFBs where both catholyte and anolyte need to possess the same charge; and 5) they still retain the scalable energy storage function.

To date there have been very few examples of reported desalination RFBs, and only at the concept stage.[16–18] These first attempts show promising ability as desalinators, with energy efficiency of <15 KJ mol^{-1} of salt removed.[16–18] However, simple metal salts ($ZnCl_2$, VCl_2, and NaI) used as charge storage materials in these reported desalination RFBs are subject to the issue of membrane crossover which causes irreversible capacity loss, thus reducing the cycling life of these desalination RFBs. In addition, high cell resistance of these systems limits the current density available to <2 mA cm^{-2}. This current density is too low for practical energy storage and desalination. Moreover, the Zn system using the solid $Zn^{2+/0}$ redox chemistry loses the flexibility of standard all-flow RFBs including tunable storage, desalination capacity, and easy maintenance. Vanadium and iodide elements are not abundant enough for wide-spread applications. Based on these limitations, there is a significant opportunity to employ molecular engineering and cell design to improve performance both in terms of integrated energy storage and desalination capability.

Recently sustainable, structurally tunable redox active organic and organometallic molecules have been increasingly populated as charge storage electrolyte materials in both aqueous[19–40] and nonaqueous redox flow batteries.[41–51] We and others have made contributions to the development of pH neutral aqueous organic redox flow batteries (AORFBs) for safe and low cost large-scale and residential energy storage using sustainable, noncorrosive, nonflammable aqueous redox-active organic electrolytes and low cost ion exchange membranes.[11–14] Specifically, pH neutral AORFBs employing water-soluble, structurally tunable viologen (anolyte), TEMPO (catholyte), ferrocene (catholyte), and ferrocyanide active materials have been extensively demonstrated.[19–26] We have envisaged pH neutral AORFBs with their stable cycling performance and noncorrosive nature are the most suitable system for coupled energy storage and desalination functions. As shown in Figure 2B, these pH neutral AORFBs with their tunable and robust

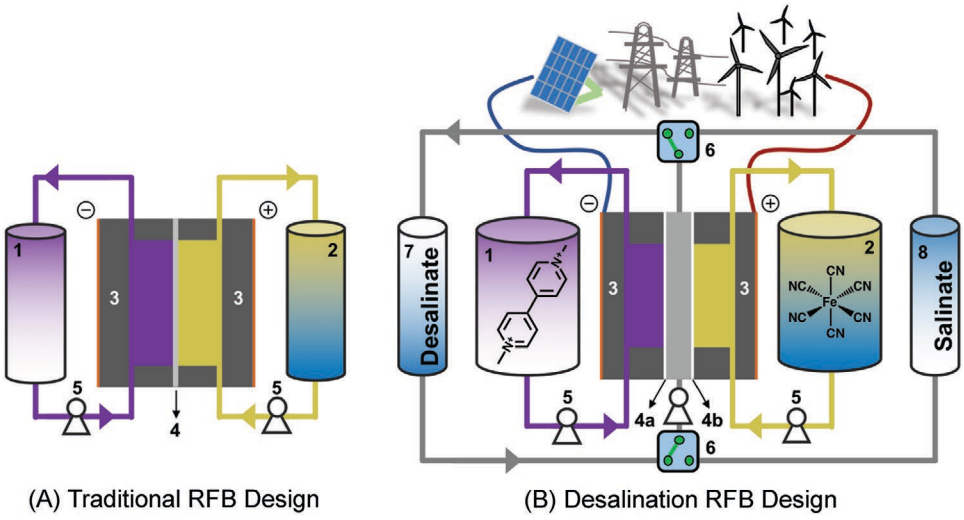

Figure 2. Graphic representation of A) traditional RFB design and the B) desalination RFB design with their cell components labeled. 1) Anolyte reservoir; 2) Catholyte reservoir; 3) Carbon electrodes; 4) Ion exchange membrane (4a for anion exchange membrane (AEM) and 4b for cation exchange membrane (CEM)); 5) Pumps; 6) Three-way switch; 7) Reservoir for desalinated water; 8) Reservoir for concentrated brine.

organic electrolyte active materials are readily adapted into desalination AORFBs.

2. Results and Discussion

2.1. Desalination Capacities and Energy Efficiencies of the MV/$Na_4[Fe(CN)_6]$ Desalination AORFBs at Different Charge Capacities

The active materials for this cell consist of methyl viologen (MV) (–0.45 V vs NHE) anolyte and sodium ferrocyanide (+0.40 V vs NHE) catholyte as they are proven redox electrolyte materials in reported pH neutral AORFBs.[21,26,39,40] The working principle for the viologen/ferrocyanide desalination RFB is illustrated in **Figure 3**. In a traditional RFB, the MV^{2+} cation and $Fe(CN)_6^{4-}$ anion are incompatible across a single ion exchange membrane due to their charge mismatch. However, the dual membrane setup in the desalination RFB allows for MV^{2+} and $Fe(CN)_6^{4-}$ sequestration via the anion exchange and cation exchange membranes respectively. During cell charge, MV^{2+} is reduced to MV^+ and releases a Cl^- ion into the central chamber. Simultaneously, $Fe(CN)_6^{4-}$ is oxidized to $Fe(CN)_6^{3-}$ and releases a Na^+ ion into the central chamber. The central chamber generates concentrated brine during cell charge. At 100% state of charge (SOC), the brine solution is switched to a new batch of sea water. During cell discharge, the oxidation of MV and reduction of $Fe(CN)_6$ remove NaCl from the central chamber, delivering both power and desalinated seawater simultaneously. A detailed description of the cell setup is provided in the supporting information.

To examine the desalination performance of this system, the central chamber was filled with 10 mL of 0.56 M NaCl to simulate the typical salinity of seawater, which requires a theoretical total charge capacity of 150 mA h to achieve 100% desalination depth. The desalination chamber was flanked on the anode side by a Selemion AMV anion exchange membrane, and on the cathode side by a Nafion 115 cation exchange membrane. To investigate the coupled desalination and energy storage performance, three cells were constructed using 15 mL MV anolyte and Na_4FeCN_6 catholyte at increasing concentration. The first cell employed 0.1 M active materials on both anode and cathode side, followed by 0.25 and 0.50 M. On the anode side, 2.0 M NaCl supporting electrolyte was used in all three cells. On the cathode side due to the already high conductivity of Na_4FeCN_6 solutions, and the solubility limit of Na_4FeCN_6, the 0.1 M cell employed 2.0 M NaCl supporting electrolyte, the 0.25 M cell employed 1.0 M NaCl, and the 0.5 M cell did not use additional electrolyte. For all concentrations, pH was adjusted to 7 using HCl for anolyte and NaOH for catholyte before cycling. Each cell was galvanostatically cycled at 5.0 mA cm^{-2} between 0.0 V and 1.25 V. The representative charge/discharge curves at different concentrations are given in **Figure 4**A. During the charge step the central solution increased salt concentration. The brine was collected and replaced with seawater before galvanostatic discharge to 0.0 V to produce desalinated water. NaCl concentrations were calculated from measured conductivities using a calibration curve of standard NaCl solutions (see Figure S1 in the Supporting Information). At 0.10 M active material concentration, during the charge process, the cell increased the salt concentration of the center channel (Figure 3B) from 0.56 to 0.70 M. During the discharge process, the desalination RFB did not have enough capacity (40.2 mAh) to significantly displace NaCl, only achieving a desalination level of ≈24.6% (dark green bar in Figure 4B). At 5.0 mA cm^{-2}, the desalination RFB delivered an energy efficiency of 72.1% and a coulombic efficiency of nearly 100%. The data disclose that in addition to the energy consumption of desalination, the RFB still can deliver 26.6 mW h of energy for other uses. Electrochemical impedance spectra of each cell collected before cycling, after brine concentration (fully charged), and after desalination (fully discharged) show how the varying salt concentration in the central chamber affect overall cell resistance. The EIS data revealed that the cell resistance remained ≈16 Ω cm^2 regardless of state of charge (Figure 4C) which is attributed to a small conductivity change in the central chamber.

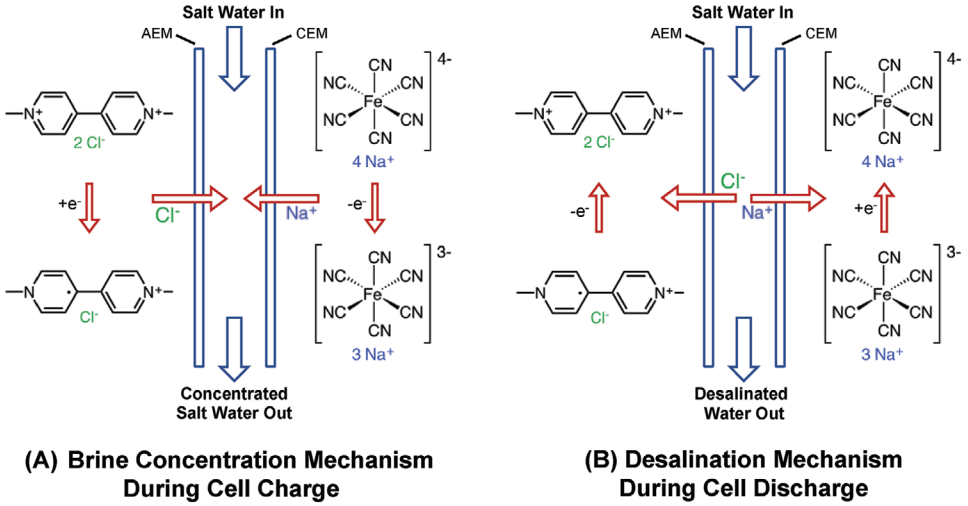

Figure 3. Working principles of desalination RFB design using methyl viologen anolyte and sodium ferrocyanide catholyte: A) salt water is concentrated during the charging process and B) salt water is desalinated during the discharging process.

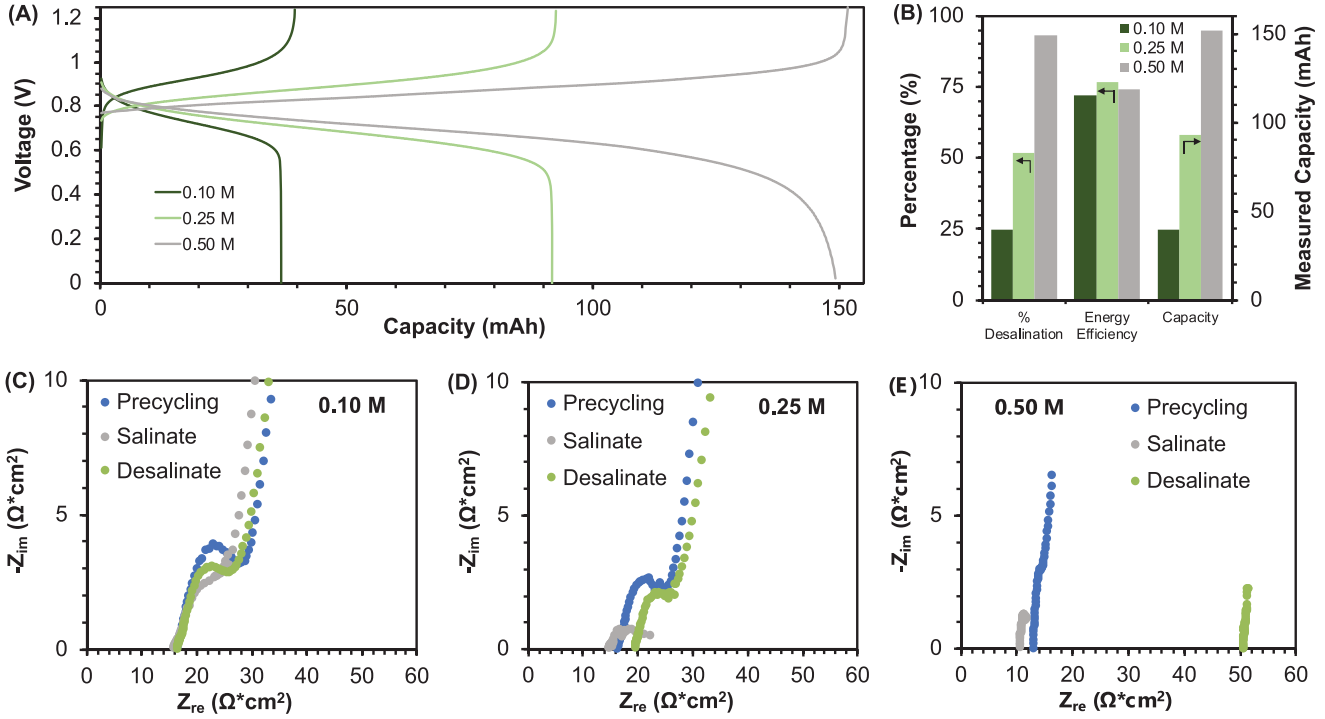

Figure 4. Cycling data and electrochemical impedance (EIS) Nyquist plots of the MV/$Fe(CN)_6$ desalination RFB. A) Charge and discharge curves of the RFB at varying concentration of active materials at 5.0 mA cm^{-2} current density. B) Percent seawater desalination, full cycle energy efficiency, and measured cell capacity plotted as functions of active material concentration. EIS Nyquist plots collected before cell cycling, after brine concentration at full cell charge, and after desalination at full cell discharge for 0.10 M C), 0.25 M D), and 0.50 M E) active materials.

By increasing the active material concentration to 0.25 M, because of the increased battery capacity (100.5 mA h, Figure 4A, light green curves), the desalination depth was largely increased to ≈65.9% (92.8 mA h) after the discharge process while the brine concentration was increased to 0.91 M (Figure 4B) after the charge process. Because of the increased battery capacity, the 0.25 M battery could deliver a higher energy output of 62.9 mW h. The 0.25 M delivered a slightly higher energy efficiency of 76.7%, though it remains comparable with the 0.1 M battery. According to the EIS data for the 0.25 M desalination RFB, the increased conductivity of the central solution after brine concentration delivered a small reduction in cell resistance, while the slightly increased battery resistance after desalination is attributed to the more complete desalination. (Figure 4D).

At 0.50 M active material concentration, the cell had enough capacity to reach near complete desalination of the central chamber, down to 0.038 M NaCl or 93.2% removal at 5.0 mA cm^{-2}. The solution pH after desalination was 7.87. The 0.50 M battery retained an energy efficiency of 74.1% representing a desalination energy cost of 3.52 W h L^{-1} of fresh water, thus capable of supplying 100.4 mW h additional energy to powering other loadings, which is higher than the 0.1 and 0.25 M batteries. It is noted the extent of desalination is ultimately limited by the continuously decreasing conductivity of the central chamber. Eventually, a desalination depth of 93.2% was reached, yielding water with a salt concentration of merely 0.038 M. As seen in Figure 4E, because of the deep level desalination of the central channel, the high frequency area specific resistance of the RFB increases from 13.1 Ω cm^2 for the freshly assembled cell to more than 50 Ω cm^2 after deep discharge. Conversely, the increased conductivity of the central chamber during brine concentration causes a slight reduction of cell resistance down to 10.7 Ω cm^2 at 100% state of charge.

Because the salt concentration in the central chamber is the capacity limiting factor during discharge of the 0.50 M battery, the discharge curve shows a unique shape compared to the other curves in Figure 4A. For the 0.10 and 0.25 M cells, the final cell capacity is limited by active material concentration only, with little contribution from increasing cell resistance. This causes a more traditional sharp drop in voltage when the active material capacity is exhausted. For the 0.50 M battery, the gradually increasing central chamber resistance is the capacity limiting factor, which causes a much more gradual voltage drop-off near cell discharge.

2.2. Current Dependence of Desalination Rate and Energy Efficiency of the MV/$Na_4[Fe(CN)_6]$ Desalination AORFB

Above studies revealed the desalination depth and effective energy storage capacity of the MV/$Na_4[Fe(CN)_6]$ desalination AORFB are simultaneously impacted by the charge capacity of the battery. Next, using the 0.50 M battery with its deep level desalination capacity, we sought to examine how the operating current can affect the desalination rate or fresh water production rate and energy efficiency of the desalination battery. Upon increasing the operating current density to 10 mA cm^{-2}, the rate of fresh water production increased from

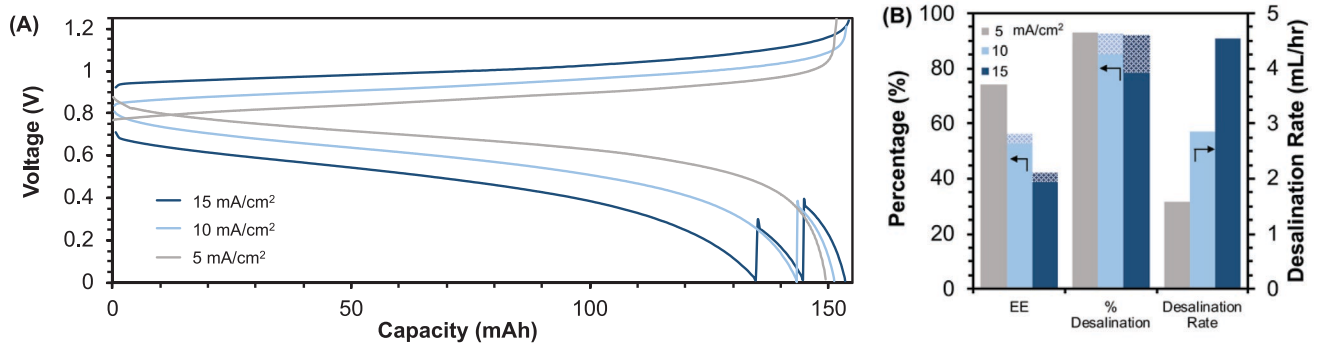

Figure 5. Charge and discharge curves of the MV + $FeCN_6$ desalination RFB collected at current densities of 5, 10, and 15 mA cm^{-2} A). At 10 mA cm^{-2}, a secondary discharge of 5 mA cm^{-2} was necessary to reach complete desalination. At 15 mA cm^{-2}, secondary and tertiary discharges of 10, and 5 mA cm^{-2} were employed. Energy efficiency (EE), % desalination, and desalination rate are plotted as functions of current density B). Desalination rate increases with current density, while EE decreases. The contribution of the additional discharge step(s) is represented by the shaded regions of the graph. The cell achieved >92% salt removal regardless of current density.

1.6 mL fresh water/hour to 2.9 mL h^{-1}, while the round trip energy efficiency decreased to 56.3% representing an energy cost 7.07 W h L^{-1} of fresh water. The increased overpotential caused the cell discharge to reach 0.0 V before complete desalination was achieved, so a secondary discharge at 5 mA cm^{-2} was employed to complete the discharge step (**Figure 5**A, light blue trace). The secondary discharge's contribution to overall performance is represented by the light shaded portions of Figure 5B. The secondary discharge step provided an additional 7.1% salt removal which allowed the cell to match the depth of desalination achieved at 5 mA cm^{-2}. Doubling the current density provided slightly less than double the rate of fresh water production due to the additional time necessary to discharge.

Further increasing the current density to 15 mA cm^{-2} sees continuations of the observed trends. The fresh water production rate increased to 4.55 mL h^{-1} at a decreased energy efficiency of 42.3% representing an energy cost of 9.06 W h L^{-1} of fresh water. The further increased overpotential during cycling necessitated a secondary discharge at 10 mA cm^{-2} and a tertiary discharge at 5 mA cm^{-2} to reach the same deep level of desalination demonstrated at the slower cycling rates (Figure 5A, dark blue trace). The data collected in the current dependent experiments is summarized in **Table 1**.

To date, this system demonstrates the fastest cycling in terms of both current density and fresh water production rate of any desalination redox flow battery. To more directly compare this cell's performance to other reported systems, the cell was also cycled at slower current density (charge at 2.5 mA cm^{-2}, discharge at 1.33 mA cm^{-2}) to more directly compare its energy efficiency to literature examples (Table 1, Figure S2, Supporting Information). Among reported desalination flow batteries ($Zn/K_4[Fe(CN)_6]$,[16] VCl_3/NaI,[17] and FMN-Na/4-HO-TEMPO[18]), the $Zn/K_4[Fe(CN)_6]$ desalination RFB represents the most efficient system truly capable of providing both power and near completely desalinated water (Table 1). Slowing the current to still twice that of the previously reported Zn system, the MV system achieves a deeper level of salt removal at a much more comparable energy cost. The combination of higher current density and larger cell capacity delivered a nearly ninefold increase in the freshwater production rate compared to the zinc system,[16] while maintaining a competitive energy efficiency compared to reverse osmosis. The slower applied current allowed for a deeper level of desalination. At a discharge current of 1.3 mA cm^{-2} the cell achieved 95.9% NaCl removal, down to 0.023 M. Our results are comparable with the energy efficiency (3–6 W h L^{-1}) and water purity of the reverse osmosis technology for sea water

Table 1. Comparison of cycling current and desalination performance between MV/$Na_4[Fe(CN)_6]$ and reported desalination RFBs.

Cell Tested	Charge Current [mA cm^{-2}]	Discharge Current [mA cm^{-2}]	Percent NaCl Removal	Energy Cost [W h L^{-1} fresh water]	Energy Cost [W h mol^{-1} NaCl removed]	Desalination Rate [mL fresh water h^{-1}]
MV/$Na_4[Fe(CN)_6]$ (this work)	15.0	15.0	92.1	9.06	17.57	4.55
"	10.0	10.0	92.4	7.07	13.66	2.86
"	5.0	5.0	93.2	3.52	6.74	1.59
"	2.6	1.4	95.9	2.40	4.47	0.60
$Zn/K_4[Fe(CN)_6]$ (Ref.13)	1.3	0.7	85	2.1	4.08	0.068
VCl_3/NaI (Ref.16)	0.22	0.22	0.42	n/a[a)]	1.49	n/a
FMN-Na/4-HO-TEMPO (Ref.17)	0.13	0.13	n/a[b)]	n/a	n/a	n/a

[a)]Due to the low percent NaCl removal, it is unreasonable to report the energy cost in units of liters of fresh water; [b)]Reference does not report the percent NaCl removal, negating energy cost calculation.

(≈0.56 M salinity) desalination[5] but at a much deeper level of desalination than other reported solid electrode based battery and capacitor deionization technologies (25–40% salt removal, Table S1).[16]

2.3. Desalination and Cycling Stabilities of the MV/$Na_4[Fe(CN)_6]$ Desalination AORFB and a Desalination Demonstration of Sea Water

To demonstrate the robust cell stability and repeatable and fast desalination performance, the 0.50 M desalination AORFB was cycled over 10 cell charge/discharge cycles for more than 60 h at 5 mA cm^{-2}. The cell first underwent a pre-charge step to bring the cell to 100% SOC, meaning the first collected data point was a discharge (desalination) step shown in green in **Figure 6**A. Charge and discharge curves from the experiment are given in Figure S3 in the Supporting Information. As shown in Figure 6, the desalination AORFB maintained a stable level of desalination at 92%. The average coulombic efficiency over the 10 cycles was more than 99.9% (Figure 6A, purple trace). Meanwhile, the average energy efficiency was retained at more than 69.0%. Moreover, post-cell analysis of MV and $Na_4[Fe(CN)_6]$ using NMR studies confirmed there was no electrolyte crossover into the central solution, which is consistent with reported stable flow battery performance of these two molecules (Figure S4, Supporting Information).[21,26,39,40]

To further demonstrate membrane and active material compatibilities, the cell's performance was tested by desalinating a sample of seawater collected from the Pacific Ocean (Depoe Bay, Oregon). As shown in Figure 6B,C, the desalination performance was very comparable to performance of the simulated solution meaning the ion selective membranes, and active materials are fully compatible with other trace ions present in real seawater. It is important to note that due to the presence of trace ions other than NaCl in seawater, the conductivity calibration curve can only approximate the salt concentration of real seawater. Nevertheless, the resulting conductivities measured during testing closely mimic the performance of the simulated seawater solution.

2.4. Cost Estimation of Scalable Fresh Water Production

It is economically interesting to make an estimation of the capital cost for fresh water production using the reported organic desalination flow battery. This device will follow the same economic trajectory predicted for traditional redox flow batteries according to our previous publications on aqueous organic redox flow batteries (see additional supporting information).[22,26]

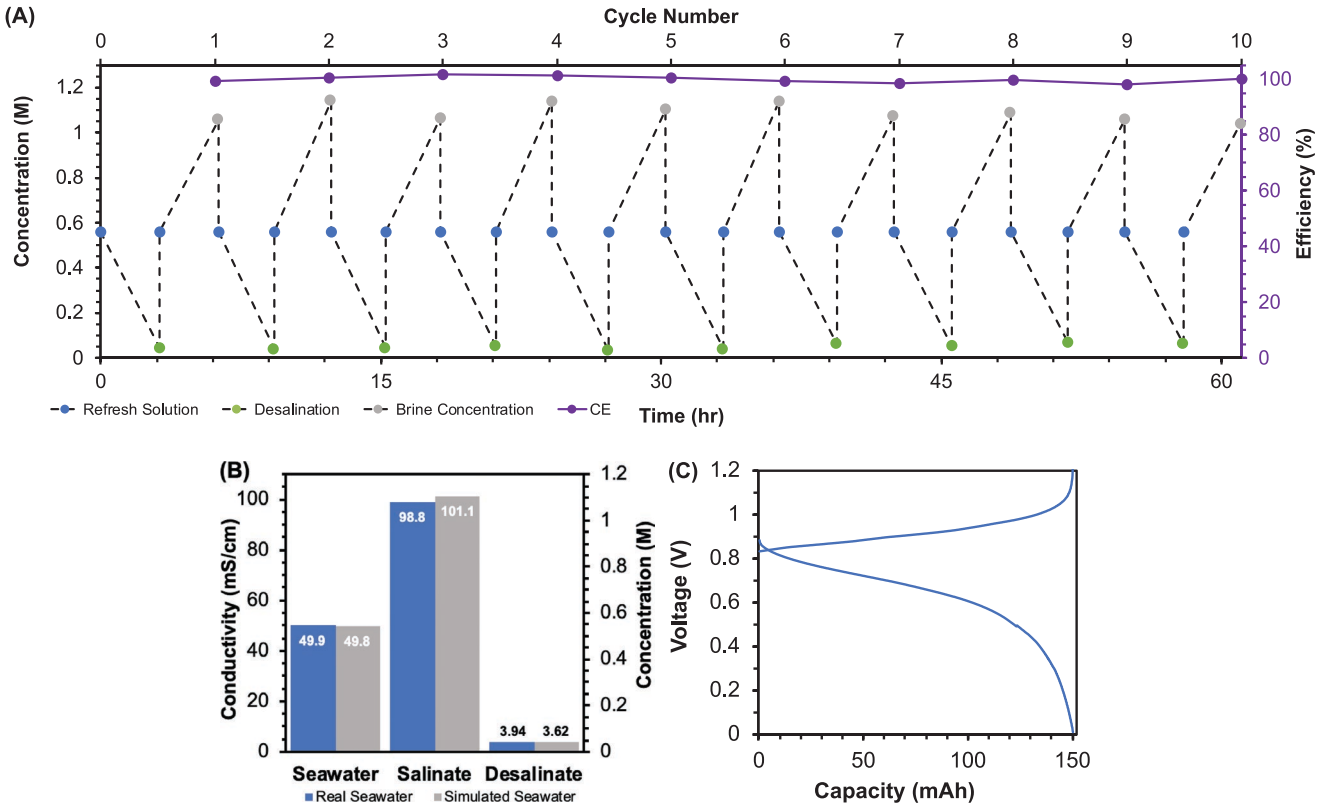

Figure 6. A) 10 cycle desalination performance at 5 mA cm^{-2}. At full discharge, the desalinated solution (green) was collected and the central RFB chamber was refreshed with seawater solution (blue). After cell charge, the concentrated brine (grey) was collected and again refreshed with seawater solution. Round trip coulombic efficiencies are reported for each cycle (purple). B) Comparison of the starting conductivity measurements of real and simulated seawater, conductivities after brine concentration, and after desalination. The secondary y axis is calibrated to NaCl concentration. C) Charge and discharge curves of the desalination RFB tested with actual Pacific Ocean seawater.

Materials costs of MV ($1.0 kg^{-1})[22] and sodium ferrocyanide ($1.0 kg^{-1})[26] of this desalination flow battery could be estimated around $16 kW^{-1} h^{-1}.[22] Selemion AMV is already very cost effective at ≈$50 m^{-2}, equivalent to ≈$12 kW^{-1} h^{-1}.[22] However, Nafion membrane is expensive ($500 m^{-2}), equivalent to ≈$120.7 kW^{-1} h^{-1}.[22] Other cell components (cell framework, electrodes, and pumps etc.) were estimated ≈$100 kW^{-1} h^{-1}.[22] Adding all cost together, the reported MV/$Na_4[Fe(CN)_6]$ desalination RFB has a capital cost of $248.7 kW^{-1} h^{-1}.[22] In the meanwhile, the energy cost of fresh-water production is ≈2.4 W h L^{-1}, and corresponds to a capital cost of $0.6 L^{-1}. In addition to the energy storage benefit, for fresh water production at a scale of 1000 L, the water production cost is $0.06 L^{-1}, which means a larger scale leads to a lower cost. We are currently looking into utilizing an equally low cost Selemion CSO membrane (≈$50 m^{-2}) as AMV to replace the more expensive Nafion 115. Then capital cost can be further down to ≈$140 kW^{-1} h^{-1}, and drives the cost of fresh water production down to $0.34 L^{-1} or $0.034 L^{-1} for a scale of 1000 L. This cost estimation only provides a benchmark on the scalable fresh water production using the reported organic desalination flow battery but is subject to more accurate economic analysis.

3. Conclusion

In summary, high performance aqueous RFB electrolytes methyl viologen and sodium ferrocyanide were paired together in a three-chamber dual membrane cell. Harnessing the charge balancing salt flow during charge/discharge allowed this cell to deliver coupled water desalination and energy storage. From simulated seawater (0.56 M NaCl), the RFB delivered 95.9% desalination at an energy cost as low as 2.4 W h L^{-1} of fresh water, and at demonstrated current densities up to 15 mA cm^{-2}. Simultaneous with desalination, the RFB was able to deliver reliable energy up to 79.7% energy efficiency. The desalination RFB was also shown to be fully functional with a sample of real seawater. Unlike previous reported desalination RFB studies, this desalination battery can provide more energy efficient fresh water production, and also deliver high current energy storage. It is expected that designable and tunable redox active molecules will not only enable versatile designs of desalination AORFBs but also further improve desalination and energy storage performance. As both renewable energy production and water scarcity increase, this technology's bifunctional capability offers opportunities to address both of these issues through one device.

Supporting Information

Supporting Information is available from the Wiley Online Library or from the author.

Acknowledgements

The authors thank Utah State University for providing faculty startup funds to the PI (T.L.L.) and the Utah Science Technology and Research initiative (USTAR) UTAG award for supporting this study. T.L.L. acknowledges National Science Career Award (Grant No. 1847674) for supporting a portion of research assistantship for W.W. C.D. is grateful to the USU Presidential Doctoral Research Fellowship (PDRF) program to support his Ph.D. program.

Conflict of Interest

A patent application including the results reported herein has been submitted.

Author Contributions

T.L.L. designed the project. C.D. conducted experiments. W.W., K.C., and B.V. helped on collecting and analyzing experimental data. T.L.L. and C.D. analyzed experimental data and prepared the manuscript, and all authors contributed to revising the manuscript and providing intellectual advices.

Keywords

desalination, energy storage, ferrocyanide, flow batteries, viologen

Received: January 15, 2020
Revised: March 14, 2020
Published online:

[1] R. F. Service, *Science* **2006**, *313*, 1088.
[2] M. Elimelech, W. A. Phillip, *Science* **2011**, *333*, 712.
[3] M. A. Shannon, P. W. Bohn, M. Elimelech, J. G. Georgiadis, B. J. Mariñas, A. M. Mayes, *Nature* **2008**, *452*, 301.
[4] A. D. Khawaji, I. K. Kutubkhanah, J.-M. Wie, *Desalination* **2008**, *221*, 47.
[5] A. Al-Karaghouli, L. L. Kazmerski, *Renewable Sustainable Energy Rev.* **2013**, *24*, 343.
[6] M. E. Suss, V. Presser, *Joule* **2018**, *2*, 10.
[7] L. Doman, *EIA projects 28% increase in world energy use by 2040." International energy outlook byUS Energy Information Administration*, https://www.eia.gov/todayinenergy/detail.php?id=32912 (accessed: September 2017).
[8] K. Frenken, V. Gillet, Irrigation water requirement and water withdrawal by country." FAO Aquastat Reports, http://www.fao.org/nr/water/aquastat/water_use/index.stm (accessed: 2012).
[9] *BP Statistical Review of World Energy* (68th edition), https://www.bp.com/en/global/corporate/energy-economics/statistical-review-of-world-energy.html (accessed: June 2019).
[10] B. Dunn, H. Kamath, J.-M. Tarascon, *Science* **2011**, *334*, 928.
[11] J. Winsberg, T. Hagemann, T. Janoschka, M. D. Hager, U. S. Schubert, *Angew. Chem., Int. Ed.* **2016**, *56*, 686.
[12] Y. Ding, C. Zhang, L. Zhang, Y. Zhou, G. Yu, *Chem. Soc. Rev.* **2017**, *47*, 69.
[13] B. Hu, J. Luo, C. Debruler, M. Hu, W. Wu, T. L. Liu, *Encycl. Inorg. Bioinorg. Chem.* **2019**, 1.
[14] J. Luo, B. Hu, M. Hu, Y. Zhao, T. L. Liu, *ACS Energy Lett.* **2019**, *4*, 2220.
[15] G. L. Soloveichik, *Chem. Rev.* **2015**, *115*, 11533.
[16] D. Desai, E. S. Beh, S. Sahu, V. Vedharathinam, Q. van Overmeere, C. F. de Lannoy, A. P. Jose, A. R. Völkel, J. B. Rivest, *ACS Energy Lett.* **2018**, *3*, 375.

[17] X. Hou, Q. Liang, X. Hu, Y. Zhou, Q. Ru, F. Chen, S. Hu, *Nanoscale* **2018**, *10*, 12308.
[18] Q. Liang, F. Chen, S. Wang, Q. Ru, Q. He, X. Hou, C.-y. Su, Y. Shi, *Energy Storage Mater.* **2019**, *20*, 203.
[19] T. Janoschka, N. Martin, U. Martin, C. Friebe, S. Morgenstern, H. Hiller, M. D. Hager, U. S. Schubert, *Nature* **2015**, *527*, 78.
[20] T. Liu, X. Wei, Z. Nie, V. Sprenkle, W. Wang, *Adv. Energy Mater.* **2016**, *6*, 1501449.
[21] T. Janoschka, N. Martin, M. D. Hager, U. S. Schubert, *Angew. Chem., Int. Ed.* **2016**, *55*, 14427.
[22] B. Hu, C. DeBruler, Z. Rhodes, T. L. Liu, *J. Am. Chem. Soc.* **2017**, *139*, 1207.
[23] C. DeBruler, B. Hu, J. Moss, J. Luo, T. L. Liu, *ACS Energy Lett.* **2018**, *3*, 663.
[24] C. DeBruler, B. Hu, J. Moss, X. Liu, J. Luo, Y. Sun, T. L. Liu, *Chem* **2017**, *3*, 1.
[25] E. S. Beh, D. De Porcellinis, R. L. Gracia, K. T. Xia, R. G. Gordon, M. J. Aziz, *ACS Energy Lett.* **2017**, *2*, 639.
[26] J. Luo, B. Hu, C. Debruler, Y. Bi, Y. Zhao, B. Yuan, M. Hu, W. Wu, T. L. Liu, *Joule* **2019**, *3*, 1.
[27] B. Hu, J. Luo, C. Debruler, M. Hu, W. Wu, T. L. Liu, *Encyclopedia of Inorganic and Bioinorganic Chemistry* **2019**, pp. 1–25.
[28] B. Yang, L. Hoober-Burkhardt, F. Wang, G. K. Surya Prakash, S. R. Narayanan, *J. Electrochem. Soc.* **2014**, *161*, A1371.
[29] L. Hoober-Burkhardt, S. Krishnamoorthy, B. Yang, A. Murali, A. Nirmalchandar, G. K. S. Prakash, S. R. Narayanan, *J. Electrochem. Soc.* **2017**, *164*, A600.
[30] B. Huskinson, M. P. Marshak, C. Suh, S. Er, M. R. Gerhardt, C. J. Galvin, X. Chen, A. Aspuru-Guzik, R. G. Gordon, M. J. Aziz, *Nature* **2014**, *505*, 195.
[31] D. G. Kwabi, K. Lin, Y. Ji, E. F. Kerr, M.-A. Goulet, D. De Porcellinis, D. P. Tabor, D. A. Pollack, A. Aspuru-Guzik, R. G. Gordon, M. J. Aziz, *Joule* **2018**, *2*, 1894.
[32] Z. Yang, L. Tong, D. P. Tabor, E. S. Beh, M.-A. Goulet, D. De Porcellinis, A. Aspuru-Guzik, R. G. Gordon, M. J. Aziz, *Adv. Energy Mater.* **2018**, *8*, 1702056.
[33] A. Hollas, X. Wei, V. Murugesan, Z. Nie, B. Li, D. Reed, J. Liu, V. Sprenkle, W. Wang, *Nat. Energy* **2018**, *3*, 508.
[34] J. Winsberg, C. Stolze, A. Schwenke, S. Muench, M. D. Hager, U. S. Schubert, *ACS Energy Lett.* **2017**, *2*, 411.
[35] C. S. Sevov, K. H. Hendriks, M. S. Sanford, *J. Phys. Chem. C* **2017**, *121*, 24376.
[36] W. Li, H.-C. Fu, Y. Zhao, J.-H. He, S. Jin, *Chem* **2018**, *11*, 2644.
[37] W. Li, H.-C. Fu, L. Li, M. Cabán-Acevedo, J.-H. He, S. Jin, *Angew. Chem., Int. Ed.* **2016**, *55*, 13104.
[38] W. D. McCulloch, M. Yu, Y. Wu, *ACS Energy Lett.* **2016**, *1*, 578.
[39] B. Hu, C. Seefeldt, C. DeBruler, T. Liu, *J. Mater. Chem. A* **2017**, *5*, 22137.
[40] J. Luo, A. Sam, B. Hu, C. DeBruler, X. Wei, W. Wang, T. L. Liu, *Nano Energy* **2017**, *42*, 215.
[41] X. Wei, W. Duan, J. Huang, L. Zhang, B. Li, D. Reed, W. Xu, V. Sprenkle, W. Wang, *ACS Energy Lett.* **2016**, *1*, 705.
[42] Y. Ding, Y. Li, G. Yu, *Chem* **2016**, *1*, 790.
[43] C. Zhang, Z. Niu, Y. Ding, L. Zhang, Y. Zhou, X. Guo, X. Zhang, Y. Zhao, G. Yu, *Chem* **2018**, *4*, 2814.
[44] C. Yang, G. Nikiforidis, J. Y. Park, J. Choi, Y. Luo, L. Zhang, S.-C. Wang, Y.-T. Chan, J. Lim, Z. Hou, M.-H. Baik, Y. Lee, H. R. Byon, *Adv. Energy Mater.* **2018**, *8*, 170289.
[45] S. E. Doris, A. L. Ward, A. Baskin, P. D. Frischmann, N. Gavvalapalli, E. Chénard, C. S. Sevov, D. Prendergast, J. S. Moore, B. A. Helms, *Angew. Chem., Int. Ed.* **2017**, *56*, 1595.
[46] T. Hagemann, J. Winsberg, B. Haupler, T. Janoschka, J. J. Gruber, A. Wild, U. S. Schubert, *NPG Asia Mater* **2017**, *9*, e340.
[47] C. S. Sevov, D. P. Hickey, M. E. Cook, S. G. Robinson, S. Barnett, S. D. Minteer, M. S. Sigman, M. S. Sanford, *J. Am. Chem. Soc.* **2017**, *139*, 2924.
[48] C. S. Sevov, S. K. Samaroo, M. S. Sanford, *Adv. Energy Mater.* **2017**, *7*, 1602027.
[49] J. Zhang, Z. Yang, I. A. Shkrob, R. S. Assary, S. o. Tung, B. Silcox, W. Duan, J. Zhang, C. C. Su, B. Hu, B. Pan, C. Liao, Z. Zhang, W. Wang, L. A. Curtiss, L. T. Thompson, X. Wei, L. Zhang, *Adv. Energy Mater.* **2017**, *7*, 1701272.
[50] C. Jia, F. Pan, Y. G. Zhu, Q. Huang, L. Lu, Q. Wang, *Sci. Adv.* **2015**, *1*, e1500886.
[51] Y. G. Zhu, Y. Du, C. Jia, M. Zhou, L. Fan, X. Wang, Q. Wang, *J. Am. Chem. Soc.* **2017**, *139*, 6286.